CHEMISTRY OF MATERIALS

Open Access

pubs.acs.org/cm

Article

Preprocessing Affords 3D Crystalline Poly(3-hexylthiophene) Structure

Mengting Sun, Zeyuan Sun, Yulong Zheng, Russell Kim, Aaron L. Liu, Lee J. Richter, James F. Gilchrist, and Elsa Reichmanis*

Cite This: *Chem. Mater.* 2025, 37, 2795−2805

Read Online

ACCESS | Metrics & More | Article Recommendations | Supporting Information

ABSTRACT: The aggregation and crystallization of poly(3-hexylthiophene-2,5-diyl) (P3HT), a representative active layer material used for organic field-effect transistor (OFET) applications, are influenced by the solution pretreatment and deposition process. This study explores vibration-assisted convective deposition for the fabrication of OFETs in comparison to spin coating, blade coating, and convective deposition without vibration. The ultraviolet−visible spectroscopic analysis demonstrates that convective deposition, especially assisted with vibration, leads to a greater degree of intrachain interactions, longer conjugation length, and enhanced polymer backbone planarization. When the P3HT solution is preprocessed via sonication and aging, the P3HT films exhibit J-like aggregation, and (h11) peaks can be observed through grazing-incidence wide-angle X-ray scattering, suggesting an ordered 3D crystalline structure. OFETs based on such films exhibit high mobilities (up to 0.14 $cm^2 V^{-1} s^{-1}$). The results point to the sensitivity of P3HT charge transport behavior to the intramolecular interactions and backbone planarity and further deepen our understanding of the relationship between processing, aggregates, molecular ordering, and resultant device properties.

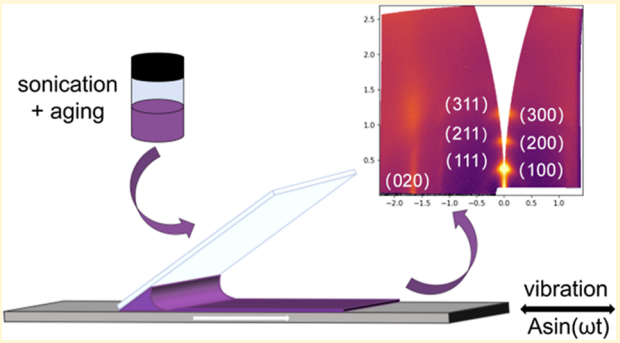

INTRODUCTION

Interest in conjugated semiconducting polymers has surged because of their vapor/solution-based processability,[1−3] compatibility with flexible substrates,[4,5] biocompatibility,[6,7] and opportunities for structural tailoring,[8,9] providing the possibility for high-performance, low-cost, and large-area electronic device fabrication.[10] These organic semiconductors (OSCs) are widely applied in various fields, including thin film transistors,[11] solar cells,[12] light-emitting diodes,[13] and sensors.[14]

OSCs still face challenges to achieve high charge transport performance due to their low crystallinity and the presence of grain boundaries, which are generated from randomly separated crystalline domains that are strongly influenced by the molecular weight.[15,16] The charge motions in OSCs are primarily governed by hopping transport,[17] which indicates that the intramolecular interactions and molecular packing play a significant role in charge transport. Many studies demonstrate that improving molecular ordering of polymer chains is desirable to increase charge carrier mobility in OSC devices.[18,19] A variety of methods to enhance both intramolecular and intermolecular interactions, including synthetic design,[20] predeposition solution treatment,[21,22] improved deposition techniques,[23,24] and postdeposition treatment,[25] have been reported to realize the desired film morphologies, ordered packing structure, and increased charge carrier mobilities. Recently, a range of preprocessing methods such as aging,[21] sonication,[26,27] ultraviolet (UV) irradiation,[22] etc., have been suggested. Specifically, studies using poly(3-hexylthiophene-2,5-diyl) (P3HT) as a model system illustrate that the polymer chains can be disentangled by sonication, facilitating the movement of polymer chains and inducing fiber nucleation through reducing the energetic barriers to form ordered nuclei.[28]

While backbone planarity and $\pi-\pi$ interactions can be enhanced by solution pretreatment,[29,30] a detailed description of the intramolecular/intermolecular interactions and how they influence charge transport remains elusive. The hopping transport model suggests that intramolecular charge transport is fastest in the direction of π-conjugation since charge carrier delocalization is mainly attributed to the electronic coupling of unhybridized p_z carbon orbitals along the backbone.[31] To date, some studies have found that transport is significantly faster

Received: December 12, 2024
Revised: March 25, 2025
Accepted: March 26, 2025
Published: April 2, 2025

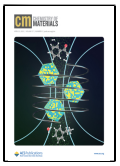

https://doi.org/10.1021/acs.chemmater.4c03392
Chem. Mater. 2025, 37, 2795−2805

along the chain axis.[32,33] The strong and direct evidence of superiority of charge transport along the backbone direction needs to be further supplemented, and the relationship between enhanced molecular interactions and their impact on device properties requires more exploration.

In this study, we demonstrate convective deposition with and without vibration assistance as an approach to create ordered OSC thin films. In conventional convective deposition, particles are assembled at the contact line of the meniscus and substrate, and films are formed via evaporation-driven flow and capillary-driven assembly of particles as the substrate moves at constant speed. This coating technique has been used to cast monolayer films from colloidal or nanoparticle systems via convective assembly.[34] An alternative convective deposition method introduces vibration of the substrate at a controlled frequency and amplitude, along with constant moving speed.[35] During this so-called vibration-assisted convective deposition process, the substrate not only keeps moving but also undergoes oscillatory in-plane vibrations. The solution experiences periodic elongation and compression, leading to unique properties of the resultant thin films. In an extension of the analysis of results obtained with colloidal particles,[35] the oscillatory motion may be expected to promote better molecular alignment and packing of polymer chains, resulting in more ordered structures. Furthermore, the vibrations influence solvent evaporation and deposition dynamics, leading to a controlled film morphology.

Here, we demonstrate the vibration-assisted coating technique as a method to cast semiconducting polymer films that exhibit enhanced charge transport properties induced through a greater degree of molecular ordering. The impact of vibration-assisted deposition was compared to convective deposition without vibration, blade coating, and spin coating on the organization of a model semiconducting polymer, P3HT. These methods were explored using solubilized semiconducting polymer solutions and sonicated solutions with and without aging. The ultraviolet−visible spectroscopy (UV−vis) results revealed that convective deposition, especially assisted with vibration, led to a greater degree of intrachain interactions, longer conjugation length, and enhanced polymer backbone planarization. When the P3HT solution was preprocessed via sonication and aging, J-like aggregation characteristics became apparent.[36] Further, (h11) peaks, which are indicative of 3D crystalline order as opposed to lamellar liquid crystalline order, were observed through grazing-incidence wide-angle X-ray scattering (GIWAXS). All devices fabricated from preprocessed solutions vs untreated controls, regardless of deposition method, exhibited similar high mobilities (up to 0.14 $cm^2\ V^{-1}\ s^{-1}$) when films were characterized using an organic field-effect transistor (OFET) platform. This study introduces vibration-assisted convective deposition as a method that can fine-tune the processes associated with thin-film formation and provides a comprehensive comparison of widely used deposition methods reported for the fabrication of organic devices. Significantly, a high degree of J-like aggregation was realized through solution treatment, leading to improved charge transport characteristics.

EXPERIMENTAL SECTION

Materials. P3HT (mass average molar mass (M_w) = 74 kDa, polydispersity (PDI) = 2.2, regioregularity = 96%) was purchased from Rieke Metals, Inc., and anhydrous chloroform was purchased from Sigma-Aldrich (≥99.8% and contains 0.5−1.0% ethanol as stabilizer). Both were used without further purification.

Solution Treatment of P3HT. P3HT solutions (5 mg/mL) were prepared in chloroform at 55 °C with stirring for 30 min. After the complete dissolution of P3HT, the solution was cooled to room temperature. The solution treatment included ultrasonication and aging. An ultrasonic cleaner (40 kHz) was used to ultrasonicate the solution for a period of 10 min. The solution exhibited a notable color change from a bright orange to a dark purple. The ultrasonicated P3HT solutions were then stored in the dark for 120 h for aging. All solution processing was done in ambient conditions.

Film Deposition. The spin coating process was conducted at a speed of 1500 rpm (1 rpm = $2\pi/60$ rad/s) for 60 s. In blade coating, the coating speed was 1 mm/s, the blade angle was 90°, and the gap was 0.2 mm. During blade coating, the solution was dispensed at the leading edge of the blade, while the substrate moved toward the opposite side of the blade. In convective deposition, the substrate moved at a speed of 1 mm/s, the blade angle was set to 45°, and the gap was less than 1 mm. In this process, the solution was dispensed at the trailing edge of the blade while the substrate moved toward the same side of the blade. In vibration-assisted convective deposition, vibrations with varying frequencies and amplitudes were applied to the substrate. All blades used in the experiments were glass slides with dimensions of 25 × 75 × 1 mm. All film deposition was done at room temperature, and no postdeposition treatments were performed.

OFET Fabrication and Characterization. The OFETs with a bottom-gate bottom-contact configuration were fabricated by using an n-doped silicon wafer as the gate electrode. A 300 nm thick layer of thermally grown SiO_2 on the wafer surface served as the gate dielectric. The 50 nm Au source and drain electrodes with 3 nm Cr as the adhesion layer were deposited via standard photolithography followed by e-beam evaporation of the corresponding metals onto the SiO_2 layer and subsequent lift-off of the photoresist masking layer. Before semiconducting layer deposition, all devices were cleaned in a plasma cleaner for 15 min to ensure the complete removal of residual photoresist and other organic contaminants. OFET fabrication was completed by depositing the pristine or preprocessed P3HT solutions onto the precleaned substrates via spin coating, blade coating, and convective deposition. All film deposition was done at room temperature, and no postdeposition treatments were performed. OFET electrical properties were investigated in a nitrogen glovebox using a semiconductor parameter analyzer after the devices were stored in the glovebox overnight. The charge-carrier mobilities were calculated in the saturation regime (V_D = −80 V) from the transfer plots of drain current (I_D) versus gate voltage (V_G) using the following equation

$$I_D = \frac{W}{2L} C_i \mu (V_G - V_{th})^2 \quad (1)$$

where W (2000 μm) and L (50 μm) are the transistor channel width and length, respectively, V_{th} is the threshold voltage, and C_i is the capacitance per unit area of the silicon dioxide gate dielectric (1.15×10^{-8} F/cm^2). The fit range is from V_G = −60 to −40 V.

UV−Vis Spectroscopy. The solid-state UV−vis spectra were obtained by an Agilent Cary 5000 spectrophotometer, which has a 175−3300 nm spectrophotometer wavelength and a 0.01−5 nm UV−vis spectral bandwidth. The corresponding P3HT films were deposited onto precleaned glass slides for all spectral measurements.

Raman Spectroscopy. Raman spectra were obtained using a Horiba LabRAM Odyssey confocal Raman microscope with a 633 nm excitation laser source in backscattering geometry, which has a 200−2200 nm measurement wavelength. The full width at half-maximum (fwhm) smaller than 0.4 cm^{-1} can be detected under such spectral resolution. The film spectra were measured through a 50× objective. The laser power was set at 50% power (8.5 mW) under all conditions to avoid photothermal effects and sample degradation. The spectral region scanned in this investigation ranged between 600 to 1799 cm^{-1}. A silicon wafer was used for the calibration process, and all spectra were collected by using LabSpec 6 software.

https://doi.org/10.1021/acs.chemmater.4c03392
Chem. Mater. 2025, 37, 2795−2805

Photoluminescence Spectroscopy. The samples were excited with a continuous wave Ar laser centered at 515 nm. All spectra were acquired using a scientific-grade, deep-cooled CCD detector coupled to an F/3.6 short-focal-length spectrograph calibrated with an Ar−Hg lamp.

Dynamic Light Scattering. DLS was carried out using an ALV/CG3 Dynamic/Static Light Scatterer at room temperature. For the instrument detection range, 0.3% mass solution was used.

Atomic Force Microscopy. The surface morphologies of the thin films were characterized by AFM using a Bruker Dimension Icon AFM system, operating in tapping mode with n-type silicon tips. The analysis of fibers was conducted via the automated image analysis tool GTFiber.[37,38]

Grazing Incidence Wide-Angle X-ray Scattering. Measurements were performed at the 11-BM CMS beamline of NSLS-II at a photon energy of 13.5 keV with the samples in a vacuum. A Pilatus 800 k detector was used. Two position stitching was performed to eliminate the horizontal gaps between detector modules. The detector distance and position of the transmission center of q-space were determined with a Ag behenate standard. The vertical position of 0,0 in q-space was empirically shifted, accounting for grazing effects, by harmonizing the (h00) series of out-of-plane diffraction. The angle of incidence was 0.12° to 0.14°. Data was analyzed using the Pygix[39] and PyFAI[40,41] packages and custom Python code.

RESULTS AND DISCUSSION

P3HT Film Fabrication in the Absence of Solution Pretreatment. Figure 1 provides a schematic representation

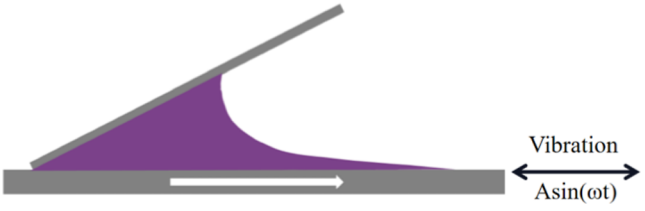

Figure 1. Schematic illustration of vibration-assisted convective deposition, where A and ω are the oscillation amplitude and angular frequency, respectively. $\omega = 2\pi f$ and f is the ordinary frequency.

of the convective deposition process, whereby the substrate moves horizontally at a set speed in conjunction with oscillatory in-plane vibrations in the direction of the deposition. The substrate translation is reversed as compared to conventional blade-coating. The film is deposited from the receding contact angle of the solution, and a 45° blade angle was used to effectively pin the solution on the receding side of the blade. The film is formed on the substrate via evaporation of the solvent. A comparison of the UV−vis spectra of P3HT films fabricated by spin coating, blade coating, normal convective deposition without vibration assistance, or convective deposition with vibration (frequency = 400 Hz, amplitude = 5 $V_{peak\text{-}to\text{-}peak}$) is presented in Figure 2a. At 400 Hz and 5 $V_{peak-peak}$, the corresponding oscillation amplitude is 3 μm, which was characterized by a high-speed confocal microscope. The absorption bands around 605 and 550 nm represent the P3HT 0−0 and 0−1 vibronic transitions, respectively. Within the weakly coupled H-aggregate model of Spano,[36] the variation of the 0−0/0−1 ratio indicates the extent of intrachain and interchain interactions. Specifically, a larger 0−0/0−1 ratio suggests enhanced intrachain interactions and/or reduced disorder, thus more J-aggregate characteristics. Therefore, the bands around 550 nm were normalized to gain insight into differences in P3HT intrachain vs interchain interactions induced through the deposition process: convective deposition leads to increased relative 0−0 band intensity with an obvious overall red-shift, which indicates increased intrachain interactions, longer conjugation length, and enhanced planarization of the polythiophene backbone.[36,42] Compared with spin coating, the 0−1 peak red-shifts from 543 to 560 nm for films obtained using the vibration-assisted process. Among the methods investigated here, vibration-assisted convective deposition leads to the highest relative amplitude of the 0−0 transition, suggesting the potential for improved charge transport characteristics and high-performance devices.[36,42]

Figure 2b focuses on the two main P3HT in-plane ring skeleton Raman modes at ∼1445 cm^{-1} (symmetric C═C stretching mode) and ∼1381 cm^{-1} (C−C intra-ring stretching mode). The more ordered P3HT phase can be identified by (1) a shift to lower wavenumber for the C═C mode peak position, (2) a narrower fwhm of the C═C mode, and (3) a larger intensity of the C−C mode with respect to the C═C mode.[43] The vibration-assisted convective deposition has the narrowest C═C mode peak fwhm (∼26.8 cm^{-1}) and the highest $I_{c-c}/I_{c=c}$ ratio (∼0.15), suggesting an enhancement in molecular order. Even though the changes in the Raman spectra are small, the trend of obtaining a narrower fwhm of the C═C mode and a higher ratio $I_{c-c}/I_{c=c}$ remains consistent. The analysis of Raman data can be considered as supportive evidence for results obtained from the UV−vis analysis.

Given the favorable UV−vis and Raman spectroscopic results, suggesting that vibration-assisted convective deposition leads to more ordered semiconducting polymer films with possibly commensurate charge transport characteristics, the coating process parameter space was explored from the perspectives of frequency and amplitude. The mobility differences obtained for OFETs fabricated using different deposition parameters are illustrated in Figure 2c and provided in Table S1. Mobility, used here as a measure of charge transport, initially improves with an increase of frequency and amplitude but then decreases. The 3D colormap distinctly identifies a frequency of 400 Hz and an amplitude of 5 V_{p-p} as the optimum point that provides for devices exhibiting the highest mobility among all the combinations, namely, up to 0.023 $cm^2\ V^{-1}\ s^{-1}$. The results suggest that vibration-assisted convective deposition offers a tunable, one-step method to achieve a higher degree of P3HT backbone planarization, leading to increased charge carrier mobility. As shown in Figure 2d, in comparison to the alternative deposition approaches investigated here, vibration-assisted convective deposition provides for devices exhibiting the highest mobility (0.023 $cm^2\ V^{-1}\ s^{-1}$), which represents a 15-fold increase vs spin-coated analogues and is a result consistent with UV−vis and Raman analysis.

P3HT Film Fabrication from Pretreated Solutions. *Photophysical Characteristics.* Figure 3a demonstrates that subjecting the as-prepared P3HT solutions to sonication (10 min), followed by aging for 120 h, promotes the formation of P3HT aggregates. The enhanced 0−0 transition and overall red-shifted spectra suggest a more planarized chain backbone. For instance, the 0−1 vibronic band shifted from 543 to 562 nm when the films were prepared via spin-coating from pristine and preprocessed solutions, respectively. Among all preprocessed cases, vibration-assisted convective deposition affords films exhibiting the most significant red shift of the 0−1 peak,

https://doi.org/10.1021/acs.chemmater.4c03392
Chem. Mater. 2025, 37, 2795−2805

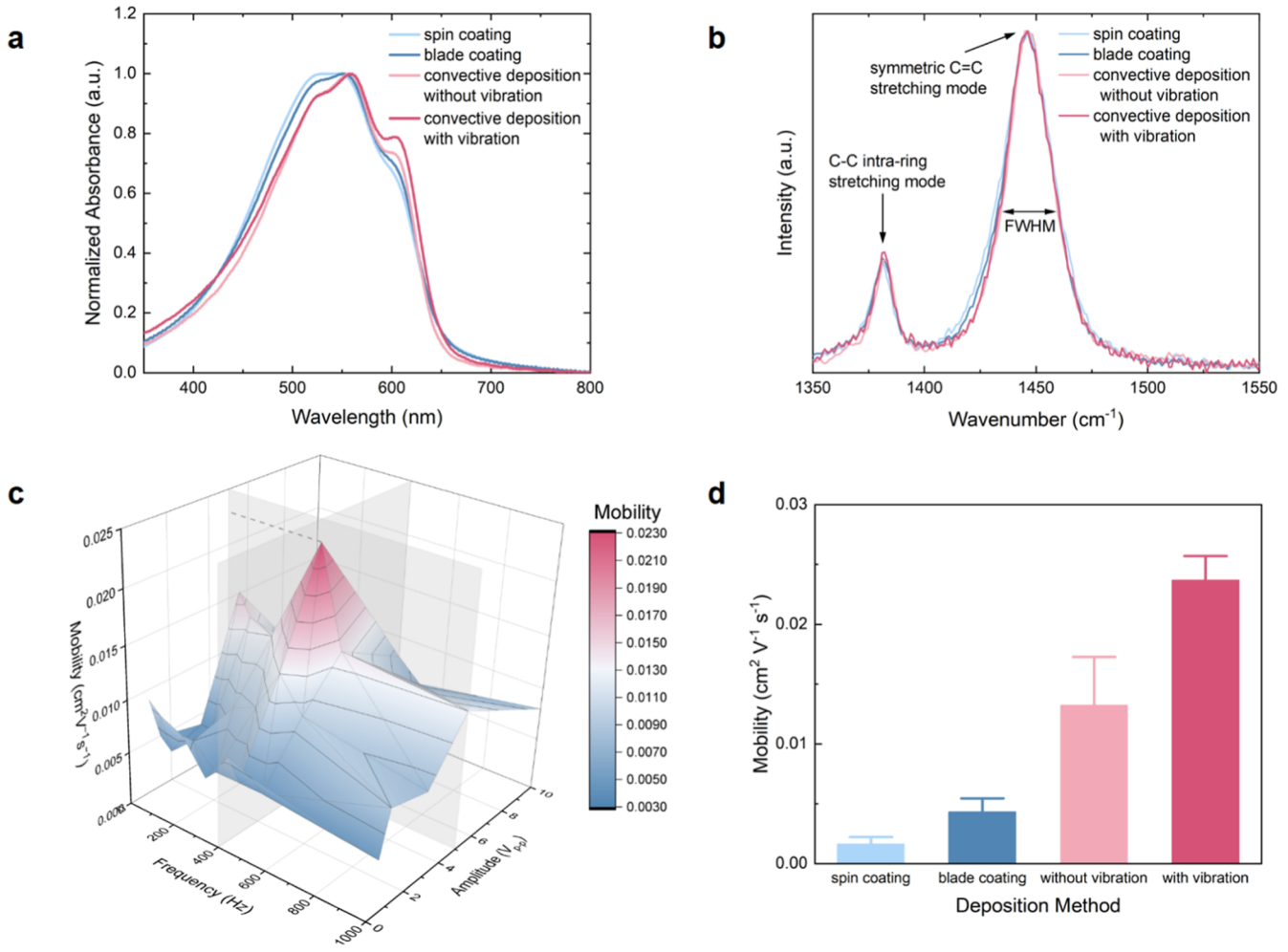

Figure 2. (a) UV−vis and (b) Raman spectra of P3HT films cast by different deposition methods. (c) 3D colormap of mobilities of P3HT films cast by vibration-assisted convective deposition with different frequencies and amplitudes. The gray areas represent the auxiliary planes at frequency = 400 Hz and amplitude = 5 V_{p-p}. The auxiliary line points to mobility = 0.023 $cm^2 V^{-1} s^{-1}$. (d) Average field-effect mobilities of P3HT films cast by different deposition methods. In the convective deposition with vibration, the applied frequency is 400 Hz and the amplitude is 5 V_{p-p}. Error bars are the standard deviation of the mean for a minimum of 5 devices.

which appears at 566 nm. Raman spectral results (Figure 3b) provide additional evidence that convective deposition leads to a more ordered P3HT phase. As shown by Silva and Spano, when the intensity ratio of the 0−0 to 0−1 vibronic features, R, exceeds 1, P3HT exhibits J-like aggregation and a change in sign of the interchain coupling.[36] In the Spano model, the distinction between *H*- and J-aggregation is strictly determined by the sign of the interchain excitonic coupling (J). *H*-aggregation occurs when the excitonic coupling is positive ($J > 0$), leading to a blue shift in the absorption spectrum due to face-to-face molecular stacking, which suppresses the 0−0 transition. *J*-aggregation occurs when the excitonic coupling is negative ($J < 0$), resulting in a red shift due to head-to-tail dipole alignment, which enhances the 0−0 transition. This change in the nature of interchain coupling is attributed to an increase in backbone planarity and stronger intrachain interactions.[44] From Figure 3c, R is greater than 1 (J-like) in the case of blade coating and convective deposition (with and without vibration-assistance) but remains less than 1 (H-like) when films are obtained via spin-coating. Notably, vibration-assisted convective deposition leads to films having the greatest R. The J-like behavior is subtle, as PL results (Figure S1) indicate predominant *H*-like aggregate behavior of the emitting state for all P3HT film samples, where interchain excitonic coupling is dominant.[45,46]

The impact of the sonication time on the UV−vis characteristics of the various P3HT films is illustrated in Figure S2. As shown in Figure S2b, R increases asymptotically with sonication time but always remains lower than 1. Presumably, as sonication time increases, the process continues to induce nucleation of P3HT aggregates, which upon aging grow into long fibrillar structures. However, as evidenced by observed changes in the UV−vis 0−0 vibronic band, the system approaches saturation at about 10 min. Conceivably, within 10 min, polymer chain disentanglement has been maximized and small P3HT aggregates have formed throughout the solutions. DLS provides additional insight, where the results indicate that the particle sizes generally decrease after sonication as a result of disentanglement (Figures S3 and S4).

The intramolecular and intermolecular ordering of the polymer chains was analyzed quantitatively using the Spano model.[47,48] The ratio R of the 0−0 and 0−1 vibronic bands is correlated with the free exciton bandwidth (W), which in turn correlates with intrachain ordering along an individual polymer chain.[42,44] A decrease in W indicates enhanced intrachain

https://doi.org/10.1021/acs.chemmater.4c03392
Chem. Mater. 2025, 37, 2795−2805

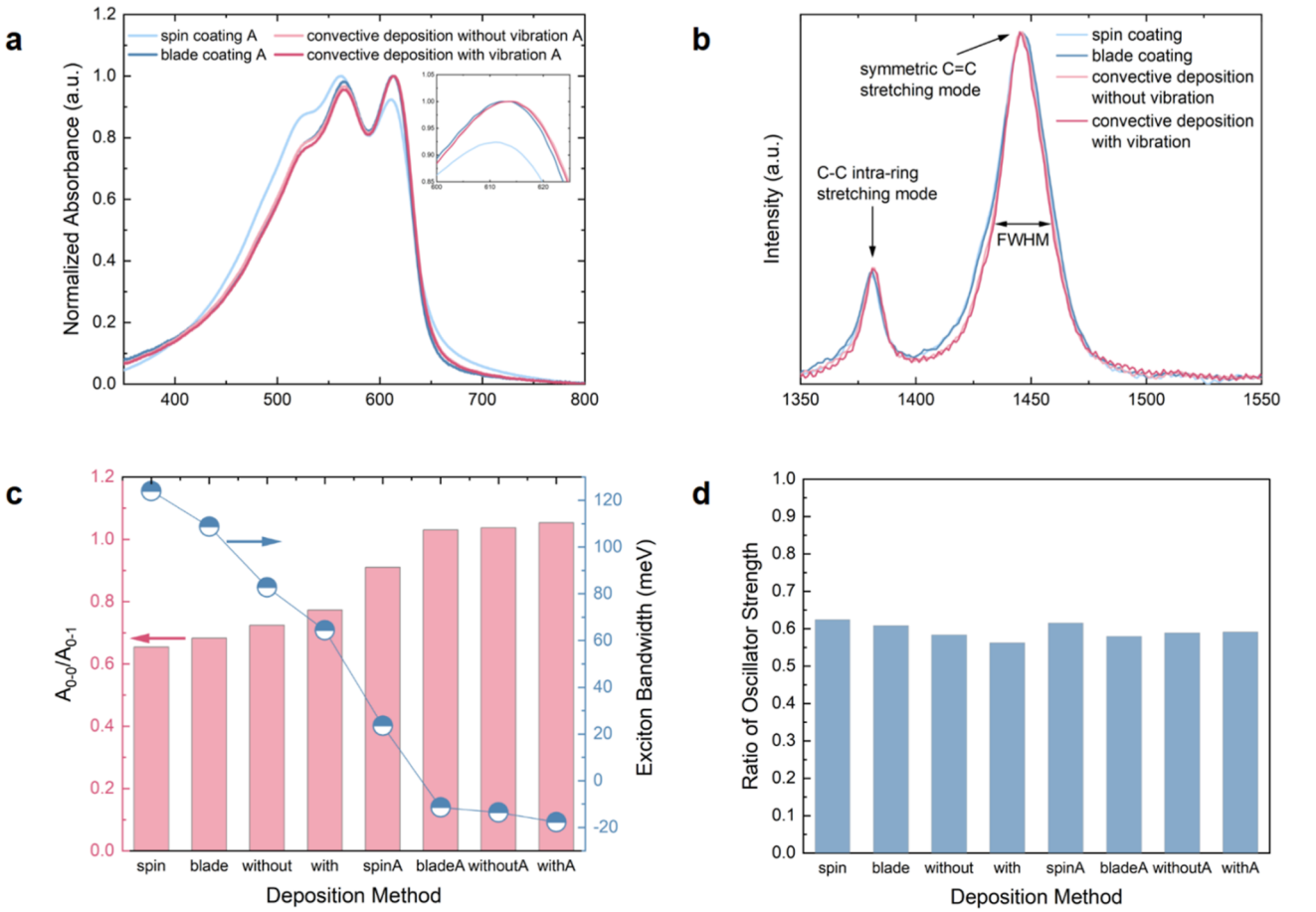

Figure 3. (a) UV−vis spectra of P3HT films cast from sonicated and aged solutions using different deposition methods. The zoom-in image shows the region of 600 to 625 nm. (b) Raman spectra of P3HT films cast from sonicated and aged solutions using different deposition methods. (c) Ratios of the 0−0 and 0−1 vibronic bands and free exciton bandwidth calculated from the film spectra using the Spano model (lambda = 1).[47,48] (d) Ratio of oscillation strength calculated from the aggregate absorbance obtained from the Franck−Condon fits (lambda = 1). "Without" refers to convective deposition without vibration and "with" means vibration-assisted convective deposition. The suffix "A" refers to samples cast from preprocessed solutions.

excitonic interactions, suggesting increased average conjugation length along with better intramolecular ordering.[27] As indicated in Figure 3c, both the deposition method and solution treatment can affect aggregate characteristics. From the perspective of deposition method, films fabricated from spin-coated pristine P3HT solutions exhibit a W of 119 meV, while those cast via vibration-assisted convective deposition have a significantly lower *W* of 62 meV, which is in the range reported for preprocessed P3HT solutions.[25,49,50] After preprocessing, blade coating and both convective deposition approaches afford *R* values above 1, suggesting *J*-like aggregation, and *W* decreases significantly. It is important to note that in the cases where *R* is > 1, *W* becomes negative, and that the Spano model was established to demonstrate *H*-like aggregation. Nevertheless, the films in question here tend to exhibit significant *J*-like aggregation. The observed reductions in exciton bandwidth point to increased conjugation along the polymer backbone due to enhanced intramolecular ordering, particularly for films fabricated by using vibration-assisted convective deposition.

To investigate the proportion of aggregates and nonaggregates in the respective films, the ratio of oscillator strength (Figure 3d) was calculated from the aggregate absorbances obtained from the Franck−Condon fits (Figure S5).[47,51] Previously, Clark et al. estimated the degree of aggregation by calculating the ratio of the aggregates and nonaggregates integrated absorption (or oscillator strength) partitioned by the molar extinction coefficients, assuming that the polymer chains transition fully between aggregates and nonaggregates during aggregation or dissolution.[42] Given that the distribution of *H*- and *J*-aggregates is comparable in our system, along with the presence of nonaggregates, accurately determining their respective absorption coefficients becomes challenging.[52] As a result, a higher ratio of oscillator strength need not be equal to a higher degree of aggregation. Additionally, differences in the degree of in-plane orientation will influence the ratio. The ratio of oscillator strength here enables the interpretation of the results relative to each other. From the analysis presented in Figure 3d, preprocessing the polymer solution does not appear to have a significant impact on the ratio of oscillation strength. The slight decrease in the ratio of oscillator strength for the pristine vs sonicated and aged solution alternatives is likely due to differences in not only the *J*- and *H*-aggregate ratios but also their absorption coefficients. Overall, analysis of the ratio of oscillator strength in conjunction with ratio *R* suggests that the deposition methods and solution treatments used in this study have a pronounced impact on P3HT aggregation behavior, demon-

https://doi.org/10.1021/acs.chemmater.4c03392
Chem. Mater. 2025, 37, 2795−2805

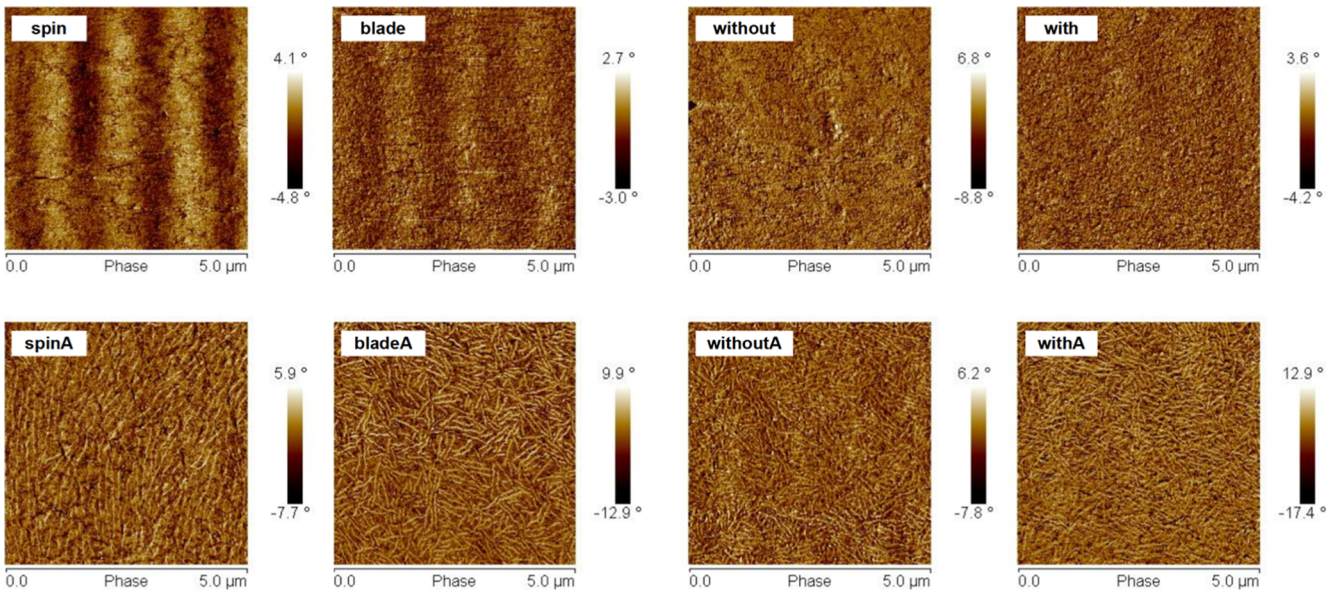

Figure 4. AFM phase images of P3HT films cast from the pristine and preprocessed solutions using different deposition methods. "Without" refers to convective deposition without vibration and "with" means vibration-assisted convective deposition. The suffix "A" refers to samples cast from preprocessed solutions.

strating changes in the tendency of the conjugated polymer to form *J*- and/or *H*-aggregate structures.

Characterization of Surface Morphology. The film surface morphologies were investigated by tapping mode AFM, with the respective phase images (5 × 5) μm, presented in Figure 4. Nanofibrillar structures are not evident in films fabricated from pristine P3HT solutions (top images in Figure 4), while fibrillar structures are clearly apparent in films cast from preprocessed solutions (bottom images in Figure 4) most likely due to a higher proportion of aggregates and longer fibers. The fiber characteristics were analyzed by GTFiber.[37,38] The fiber length density (ρ_{FL}) is the total length of fibers per unit area, capturing the packing density of fibers and revealing the long-range structure.[38] Table S3 suggests that vibration-assisted convective deposition afforded the highest fiber length density, which may serve to enhance charge transport. All the samples showed large fiber width but shorter fiber length than samples that were only aged or obtained with shorter sonication time in the previous study.[27] The results can be understood from the perspective of crystallization mechanisms. During self-assembly of P3HT into fibers, the primary driving force for growth is the physical $\pi-\pi$ stacking interaction.[53] Sonication helps disentangle polymer chains, inducing fiber nucleation through reducing the energetic barrier to form ordered nuclei,[28] and aging enables sufficient time for the formation of relatively long fibers. Even though the disentanglement of polymer chains induced by sonication facilitates aggregation, the aggregates are more dispersed and smaller, which results in shorter fibers. The presence of rotational freedom increased by sonication also limits the formation of long fibers.

P3HT Film Crystallinity. Since it is accepted that charge transport is most efficient in the ordered crystalline regions of conjugated polymer films,[19] the packing structure and organization of P3HT chains in the as-fabricated samples were investigated by GIWAXS (Figure 5).

Diffraction peaks associated with lamellar stacking (100, 200, and 300) along the q_z direction and the peak (020) related to $\pi-\pi$ stacking along the q_{xy} direction are apparent in all films. Here, it was assumed that $Z = 2$ and $P2_1/c$ for the P3HT crystal structure,[54] and then the (020) signal was used to mark the $\pi-\pi$ stacking peak at ∼1.7 Å^{-1}. The observation of these peaks suggests an edge-on orientation. Furthermore, blade coating and convective deposition appear to afford films with more orientationally ordered crystalline regions vs spin coating, where the spin-coated samples point to isotropic character in both the out-of-plane and in-plane directions (the ring pattern presents with uniform intensity). In contrast, films prepared from preprocessed solutions exhibit clearer, higher-order stacking peaks, indicating enhanced molecular ordering. Enhanced crystallinity due to preprocessing is also clear in the relative degree of crystallinity, as shown in Figure S8. The unexpectedly high relative degree of crystallinity observed in the spin-coated samples is likely attributed to the relatively greater film thickness. Surprisingly, the (h11) peak series (as labeled in Figure 5a) is observed clearly in films cast from preprocessed solutions and supports the hypothesis that the P3HT crystal structure follows $Z = 2$ and $P2_1/c$. Note, the odd order reflection for both (00*l*) and (0*k*0) are forbidden in $P2_1/c$.[54] Additionally, the (001) and (010) are nearly degenerate; thus, assessment of chain director (001) order is difficult. The observation here of (h11) suggests that the structures possess 3D crystalline order as opposed to lamellar, liquid crystalline order. Only films cast from preprocessed solutions exhibit clear (h11) peaks regardless of deposition methods, indicating that the appearance of (h11) peaks is primarily attributed to the solution treatment. Conceivably, solution preprocessing leads to J-like aggregation, which, in turn, enhances backbone planarity and molecular ordering. Concomitant increased intermolecular interactions result in the appearance of the (h11) peaks.

Figure 5b allows for additional analysis of the molecular stacking. The lamellar stacking distances d_{100} were calculated using Bragg's law, and the positions of (100) diffraction peaks (∼0.4 Å) and the $\pi-\pi$ stacking distances d_{020} were derived from the positions of (020) diffraction peaks (∼1.7 Å). The

https://doi.org/10.1021/acs.chemmater.4c03392
Chem. Mater. 2025, 37, 2795−2805

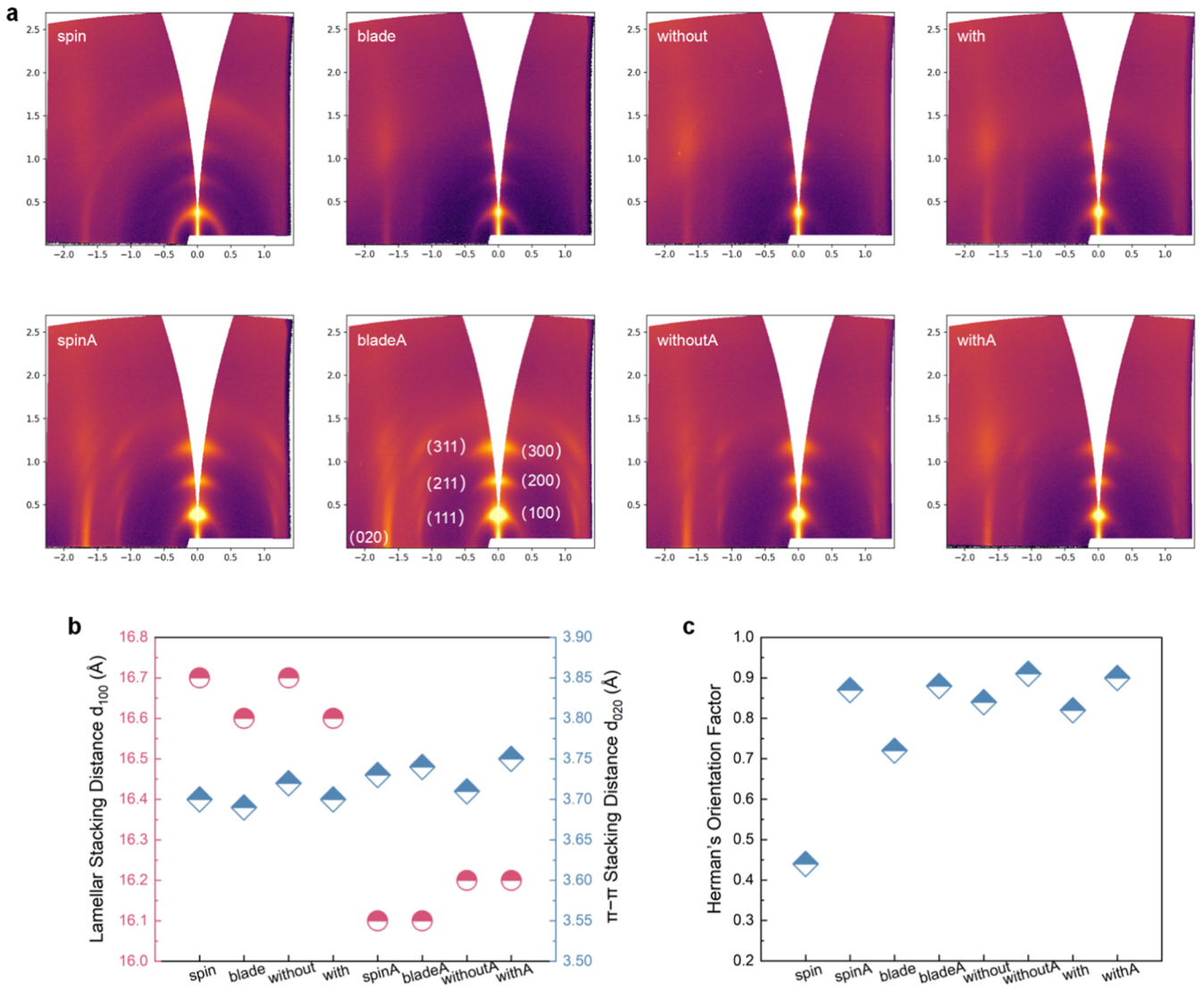

Figure 5. (a) GIWAXS patterns of P3HT films cast from the pristine and preprocessed solutions using different deposition methods. For all GIWAXS images, the X axis is "q_{xy} (Å^{-1})" and the Y axis is "q_z (Å^{-1})". (b) Calculations of lamellar stacking distance and $\pi-\pi$ stacking distance for all samples. (c) Calculations of Herman's orientation factor for all samples. "Without" refers to convective deposition without vibration and "with" means vibration-assisted convective deposition. The suffix "A" refers to samples cast from preprocessed solutions.

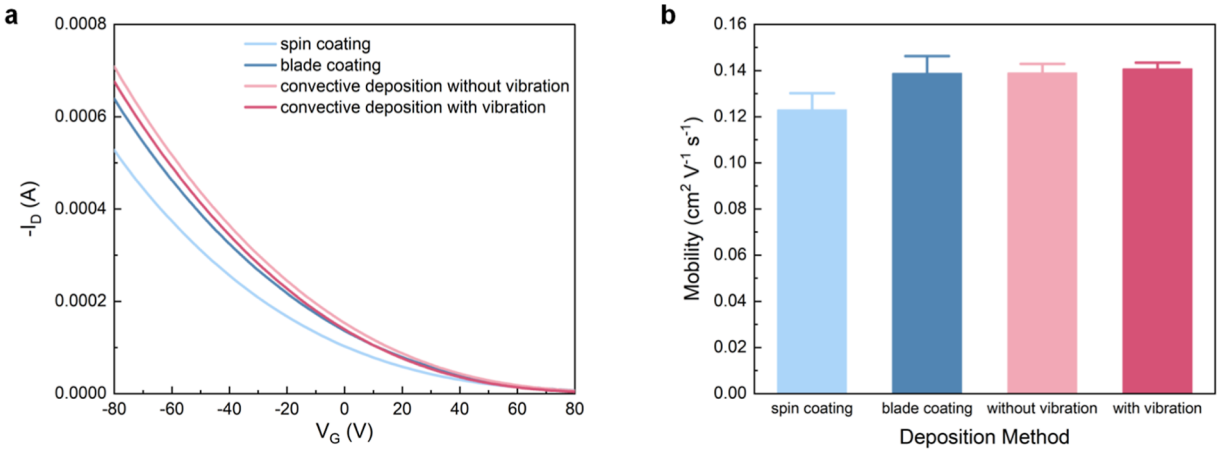

Figure 6. (a) Transfer characteristics and (b) average field-effect mobilities of P3HT films cast from preprocessed solutions using different deposition methods. Error bars are the standard deviation of the mean for a minimum of 5 devices.

https://doi.org/10.1021/acs.chemmater.4c03392
Chem. Mater. 2025, 37, 2795−2805

results indicate that the deposition method has only a limited impact on both the lamellar and $\pi-\pi$ stacking distances. On the other hand, preprocessing the solutions decreases the lamellar stacking distances from ∼16.6 to ∼16.1 Å, indicating better lamellar stacking and enhanced ordering along the out-of-plane direction. Preprocessing, however, does not appear to affect the $\pi-\pi$ stacking. To estimate the crystal orientation and quantify the alignment of a given axis, the Herman's orientation factor, f_H, was calculated. The f_H can range from −0.5 (indicating a lattice plane oriented perfectly parallel to the substrate or face-on) to 1 (suggesting crystal planes oriented perfectly perpendicular to the substrate or edge-on). The f_H equals 0 when randomly oriented structures exist. Except for the samples spin-coated from pristine solutions, all thin films show a highly oriented edge-on character. It can be deduced that the solution treatment is an efficient way to improve the crystal orientation, and convective deposition also serves a positive role in increasing the crystal orientation.

A qualitative correlation has been established between the $\pi-\pi$ paracrystallinity (g parameter) and intrachain order.[19,55] As shown in Table S6, the g parameter was estimated from the (020) diffraction width (assuming no contribution from the (002) and thus an upper bound). As shown in Figure S9, there is a clear correlation between the g parameter and the interchain coupling, W, from the UV−vis analysis, reinforcing the attribution of the weaker interchain coupling to enhanced intrachain order.

Device Properties. As indicated in Figure 6, all samples fabricated from preprocessed P3HT solutions exhibit similar improved mobility. In the four film fabrication methods used in this study, the mobilities of the blade-coated and convective deposition samples are almost the same (up to 0.14 $cm^2\ V^{-1}\ s^{-1}$). The mobility is outstanding among present studies and represents a significant increase compared to films fabricated in the absence of preprocessing (7-fold increase with respect to spin-coated samples). Thus, solution preprocessing supports the organization of P3HT into fibers that are favorable for enhanced charge carrier transport. We note that the devices exhibit a significant threshold voltage (independent of solution pretreatment), suggestive of trapped charges in the dielectric. Nonetheless, the saturation behavior of eq 1 is followed (Figure S18).

The changes in lamellar stacking are limited, and many previous works have achieved similar results.[27,56,57] Also, the P3HT alkyl chain direction does not contribute significantly to charge transport. Since the UV−vis results indicate the solution treatment does not affect the ratio of oscillator strength significantly and GIWAXS data show its effects on crystal orientation are slight, we attribute the enhanced mobilities to the improved intramolecular order as evidenced by the increased proportion of *J*-aggregate behavior and decrease in $\pi-\pi$ g parameter. The results strongly and directly point to charge transport along the conjugated backbone as the dominant factor in transport performance, consistent with studies of aligned polymers;[23,58] and increasing the backbone planarity is a key point to improve the device properties. It also advances the exploration of the relationship between processing, molecular ordering, and charge transport through the characterization of films and devices.

CONCLUSIONS

In this study, four deposition methods (spin coating, blade coating, convective deposition without vibration, and vibration-assisted convective deposition) and solution treatment (sonication and aging) were carried out to explore how the processing and molecular interactions influence resultant conjugated polymer thin-film properties and device mobilities. The results indicate that convective deposition is favorable to induce intrachain interactions and enhance OFET performance. With solution treatment, UV−vis spectra demonstrate that P3HT films show *J*-like aggregation due to the disentanglement of polymer chains induced by sonication. The ratio $R > 1$ and decreasing W suggest increased conjugation along the polymer backbone and enhanced intramolecular ordering for films that were deposited from preprocessed solutions. The GIWAXS presents a mixed (h11) peak series, which indicates the presence of 3D crystalline order. Also, the devices fabricated from preprocessed solutions exhibit high mobilities (up to 0.14 $cm^2\ V^{-1}\ s^{-1}$).

This work applies a one-step deposition method, vibration-assisted convective deposition, and provides a promising way to control the film properties. Importantly, through the exploration of preprocessed thin-film characteristics, the understanding of the significance of molecular interactions in conjugated polymers has been deepened. In particular, *J*-aggregates facilitate necessary intramolecular interactions and backbone planarity, which play a decisive role in charge transport, and their formation can be manipulated through processing as-prepared polymer solutions prior to thin-film deposition. Combined, the findings reported here will promote further development of conjugated polymer candidates for high-performance, conjugated polymer-based devices.

ASSOCIATED CONTENT

Supporting Information

The Supporting Information is available free of charge at https://pubs.acs.org/doi/10.1021/acs.chemmater.4c03392.

Mobilities of P3HT films cast by vibration-assisted convective deposition; PL spectra, UV−vis spectra of films prepared from solutions at different sonication times, DLS measurements, UV−vis spectra fitted by Franck−Condon fits, structural order parameters and measurements obtained from AFM, 1D-GIWAXS images, and output characteristics (PDF)

AUTHOR INFORMATION

Corresponding Author

Elsa Reichmanis − *Department of Chemical and Biomolecular Engineering, Lehigh University, Bethlehem, Pennsylvania 18015, United States;* orcid.org/0000-0002-8205-8016; Email: elr420@lehigh.edu

Authors

Mengting Sun − *Department of Chemical and Biomolecular Engineering, Lehigh University, Bethlehem, Pennsylvania 18015, United States;* orcid.org/0000-0002-8659-4131

Zeyuan Sun − *Department of Chemical and Biomolecular Engineering, Lehigh University, Bethlehem, Pennsylvania 18015, United States;* orcid.org/0000-0003-0045-2392

Yulong Zheng − *School of Chemistry and Biochemistry, Georgia Institute of Technology, Atlanta, Georgia 30332, United States;* orcid.org/0000-0001-5136-1971

Russell Kim − *Department of Chemical and Biomolecular Engineering, Lehigh University, Bethlehem, Pennsylvania 18015, United States;* orcid.org/0009-0004-2829-823X

Aaron L. Liu − *School of Chemical and Biomolecular Engineering, Georgia Institute of Technology, Atlanta, Georgia 30332, United States;* orcid.org/0000-0001-7347-5347

Lee J. Richter − *Materials Measurement Laboratory, National Institute of Standards and Technology, Gaithersburg, Maryland 20899, United States;* orcid.org/0000-0002-9433-3724

James F. Gilchrist − *Department of Chemical and Biomolecular Engineering, Lehigh University, Bethlehem, Pennsylvania 18015, United States;* orcid.org/0000-0003-2066-750X

Complete contact information is available at: https://pubs.acs.org/10.1021/acs.chemmater.4c03392

Author Contributions

The manuscript was written through contributions of all authors. All authors have given their approval to the final version of the manuscript.

Notes

The authors declare no competing financial interest.

Certain equipment, instruments, software, or materials are identified in this paper in order to specify the experimental procedure adequately. Such identification is not intended to imply recommendation or endorsement of any product or service by NIST, nor is it intended to imply that the materials or equipment identified are necessarily the best available for the purpose.

■ ACKNOWLEDGMENTS

Partial support from the National Science Foundation (Grant No. 1922111), DMREF: Collaborative Research: Achieving Multicomponent Active Materials through Synergistic Combinatorial, Informatics-enabled Materials Discovery, is gratefully acknowledged. This work was performed in part at the Georgia Tech Institute for Electronics and Nanotechnology, a member of the National Nanotechnology Coordinated Infrastructure (NNCI), which is supported by the National Science Foundation (ECCS-2025462). E.R., M.S., Z.S., R.K., and J.F.G. also appreciate access to the facilities associated with the Lehigh University Institute for Functional Materials and Devices, and the Lehigh Integrated Nanofabrication and Cleanroom Facility. J.F.G., R.K., E.R., M.S., and Z.S. acknowledge support from Lehigh University in the form of nonfederal funds, E.R. appreciates support associated with nonfederal, Carl Robert Anderson Chair funds at Lehigh University, and Y.Z. is grateful for support from the Georgia Institute of Technology. This research used the CMS 11-BM beamline of the National Synchrotron Light Source II, a U.S. DOE Office of Science User Facility operated for the DOE Office of Science by Brookhaven National Laboratory under Contract DE-SC0012704. We thank Ruipeng Li for assistance in acquiring the GIWAXS data.

■ REFERENCES

(1) Wang, S.; Peng, L.; Sun, H.; Huang, W. The future of solution processing toward organic semiconductor devices: a substrate and integration perspective. *J. Mater. Chem. C* **2022**, *10* (35), 12468−12486.

(2) Zhang, Y.; Chen, A.; Kim, M.-W.; Alaei, A.; Lee, S. S. Nanoconfining solution-processed organic semiconductors for emerging optoelectronics. *Chem. Soc. Rev.* **2021**, *50* (17), 9375−9390.

(3) Hai, T.; Feng, Z.; Sun, Y.; Wong, W.-Y.; Liang, Y.; Zhang, Q.; Lei, Y. Vapor-Phase living assembly of π-Conjugated organic semiconductors. *ACS Nano* **2022**, *16* (2), 3290−3299.

(4) Qian, Y.; Zhang, X.; Xie, L.; Qi, D.; Chandran, B. K.; Chen, X.; Huang, W. Stretchable Organic Semiconductor Devices. *Adv. Mater.* **2016**, *28* (42), 9243−9265.

(5) Khau, B. V.; Scholz, A.; Reichmanis, E. Advances and Opportunities in Development of Deformable Organic Electrochemical Transistors. *J. Mater. Chem. C* **2020**, *8* (43), 15067−15078.

(6) Inal, S.; Rivnay, J.; Suiu, A.-O.; Malliaras, G. G.; McCulloch, I. Conjugated Polymers in Bioelectronics. *Acc. Chem. Res.* **2018**, *51* (6), 1368−1376.

(7) Someya, T.; Bao, Z.; Malliaras, G. G. The Rise of Plastic Bioelectronics. *Nature* **2016**, *540* (7633), 379−385.

(8) Mei, J.; Bao, Z. Side chain engineering in Solution-Processable conjugated Polymers. *Chem. Mater.* **2014**, *26* (1), 604−615.

(9) Bronstein, H.; Nielsen, C. B.; Schroeder, B. C.; McCulloch, I. The Role of Chemical Design in the Performance of Organic Semiconductors. *Nat. Rev. Chem* **2020**, *4* (2), 66−77.

(10) Park, S.; Kim, T.; Yoon, S.; Koh, C. W.; Woo, H. Y.; Son, H. J. Progress in materials, solution processes, and Long-Term stability for Large-Area organic photovoltaics. *Adv. Mater.* **2020**, *32* (51), 2002217.

(11) Mei, J.; Diao, Y.; Appleton, A. L.; Fang, L.; Bao, Z. Integrated materials design of organic semiconductors for Field-Effect transistors. *J. Am. Chem. Soc.* **2013**, *135* (18), 6724−6746.

(12) Fu, J.; Yang, Q.; Huang, P.; Chung, S.; Cho, K.; Kan, Z.; Liu, H.; Lu, X.; Lang, Y.; Lai, H.; He, F.; Fong, P. W. K.; Lu, S.; Yang, Y.; Xiao, Z.; Li, G. Rational molecular and device design enables organic solar cells approaching 20% efficiency. *Nat. Commun.* **2024**, *15* (1), 1830.

(13) Liu, Y.; Hua, L.; Yan, S.; Ren, Z. Halogenated π-conjugated polymeric emitters with thermally activated delayed fluorescence for highly efficient polymer light emitting diodes. *Nano Energy* **2020**, *73*, 104800.

(14) Zhang, X.; Wang, B.; Huang, L.; Huang, W.; Wang, Z.; Zhu, W.; Chen, Y.; Mao, Y.; Facchetti, A.; Marks, T. J. Breath figure-derived porous semiconducting films for organic electronics. *Sci. Adv.* **2020**, *6* (13), No. eaaz1042.

(15) Pisula, W.; Zorn, M.; Chang, J. Y.; Müllen, K.; Zentel, R. Liquid Crystalline Ordering and Charge Transport in Semiconducting Materials. *Macromol. Rapid Commun.* **2009**, *30* (14), 1179−1202.

(16) Gu, K.; Snyder, C. R.; Onorato, J.; Luscombe, C. K.; Bosse, A. W.; Loo, Y.-L. Assessing the Huang-Brown description of tie chains for charge transport in conjugated polymers. *ACS Macro Lett.* **2018**, *7* (11), 1333−1338.

(17) Coropceanu, V.; Cornil, J.; Da Silva Filho, D. A.; Olivier, Y.; Silbey, R.; Brédas, J.-L. Charge transport in organic semiconductors. *Chem. Rev.* **2007**, *107* (4), 926−952.

(18) Kline, R. J.; McGehee, M. D.; Toney, M. F. Highly oriented crystals at the buried interface in polythiophene thin-film transistors. *Nat. Mater.* **2006**, *5* (3), 222−228.

(19) Noriega, R.; Rivnay, J.; Vandewal, K.; Koch, F. P. V.; Stingelin, N.; Smith, P.; Toney, M. F.; Salleo, A. A general relationship between disorder, aggregation and charge transport in conjugated polymers. *Nat. Mater.* **2013**, *12* (11), 1038−1044.

(20) Nikolka, M.; Broch, K.; Armitage, J.; Hanifi, D.; Nowack, P. J.; Venkateshvaran, D.; Sadhanala, A.; Saska, J.; Mascal, M.; Jung, S.-H.; Lee, J.; McCulloch, I.; Salleo, A.; Sirringhaus, H. High-mobility, trap-free charge transport in conjugated polymer diodes. *Nat. Commun.* **2019**, *10* (1), 2122.

(21) Kleinhenz, N.; Rosu, C.; Chatterjee, S.; Chang, M.; Nayani, K.; Xue, Z.; Kim, E.; Middlebrooks, J.; Russo, P. S.; Park, J. O.; Srinivasarao, M.; Reichmanis, E. Liquid Crystalline poly(3-hexylthiophene) solutions revisited: Role of Time-Dependent Self-Assembly. *Chem. Mater.* **2015**, *27* (7), 2687−2694.

(22) Park, J. H.; Kwon, O. J.; Kim, T.-H.; Mun, J.; Park, Y. D. Ultraviolet Irradiation Creates Morphological Order *via* Conforma-

tional Changes in Polythiophene Films. *Org. Electron.* **2018**, *62*, 394−399.
(23) Shaw, L.; Hayoz, P.; Diao, Y.; Reinspach, J. A.; To, J. W. F.; Toney, M. F.; Weitz, R. T.; Bao, Z. Direct uniaxial alignment of a Donor-Acceptor semiconducting polymer using Single-Step solution shearing. *ACS Appl. Mater. Interfaces* **2016**, *8* (14), 9285−9296.
(24) Yin, Y.; Zhu, S.; Chen, S.; Lin, Z.; Peng, J. Rapid Meniscus-Assisted Solution-Printing of conjugated block copolymers for Field-Effect transistors. *Adv. Funct. Mater.* **2021**, *32* (14), 2110824.
(25) Jang, M.; Huh, Y.-I.; Chang, M. Effects of Solvent Vapor Annealing on Morphology and Charge Transport of Poly(3-hexylthiophene) (P3HT) Films Incorporated with Preformed P3HT Nanowires. *Polymers* **2020**, *12* (5), 1188.
(26) Chang, M.; Lee, J.; Chu, P.-H.; Choi, D.; Park, B.; Reichmanis, E. Anisotropic Assembly of Conjugated Polymer Nanocrystallites for Enhanced Charge Transport. *ACS Appl. Mater. Interfaces* **2014**, *6* (23), 21541−21549.
(27) Kleinhenz, N.; Persson, N.; Xue, Z.; Chu, P. H.; Wang, G.; Yuan, Z.; McBride, M. A.; Choi, D.; Grover, M. A.; Reichmanis, E. Ordering of Poly(3-Hexylthiophene) in Solutions and Films: Effects of Fiber Length and Grain Boundaries on Anisotropy and Mobility. *Chem. Mater.* **2016**, *28* (11), 3905−3913.
(28) Zhao, K.; Khan, H. U.; Li, R.; Su, Y.; Amassian, A. Entanglement of Conjugated Polymer Chains Influences Molecular Self-Assembly and Carrier Transport. *Adv. Funct. Mater.* **2013**, *23* (48), 6024−6035.
(29) Zhao, K.; Xue, L.; Liu, J.; Gao, X.; Wu, S.; Han, Y.; Geng, Y. A New Method to Improve Poly(3-hexyl thiophene) (P3HT) Crystalline Behavior: Decreasing Chains Entanglement To Promote Order−Disorder Transformation in Solution. *Langmuir* **2010**, *26* (1), 471−477.
(30) Choi, D.; Chang, M.; Reichmanis, E. Controlled Assembly of Poly(3-hexylthiophene): Managing the Disorder to Order Transition on the Nano- through Meso-Scales. *Adv. Funct. Mater.* **2015**, *25* (6), 920−927.
(31) Salleo, A. Charge transport in polymeric transistors. *Mater. Today* **2007**, *10* (3), 38−45.
(32) Pingel, P.; Zen, A.; Abellón, R. D.; Grozema, F. C.; Siebbeles, L. D. A.; Neher, D. Temperature-Resolved local and macroscopic charge carrier transport in thin P3HT layers. *Adv. Funct. Mater.* **2010**, *20* (14), 2286−2295.
(33) Scharsich, C.; Lohwasser, R. H.; Sommer, M.; Asawapirom, U.; Scherf, U.; Thelakkat, M.; Neher, D.; Köhler, A. Control of aggregate formation in poly(3-hexylthiophene) by solvent, molecular weight, and synthetic method. *J. Polym. Sci., Part B:Polym. Phys.* **2012**, *50* (6), 442−453.
(34) Brabec, C. J.; Durrant, J. R. Solution-Processed Organic Solar Cells. *MRS Bull.* **2008**, *33* (7), 670−675.
(35) Joy, M.; Muangnapoh, T.; Snyder, M. A.; Gilchrist, J. F. Flow-induced alignment of (100) fcc thin film colloidal crystals. *Soft Matter* **2015**, *11* (36), 7092−7100.
(36) Spano, F. C.; Silva, C. H.-. H- and J-Aggregate Behavior in Polymeric Semiconductors. *Annu. Rev. Phys. Chem.* **2014**, *65* (1), 477−500.
(37) Persson, N. GTFiber2. https://github.com/Imperssonator/GTFiber2 (accessed 11 17, 2023).
(38) Persson, N. E.; Rafshoon, J.; Naghshpour, K.; Fast, T.; Chu, P.-H.; McBride, M.; Risteen, B.; Grover, M.; Reichmanis, E. High-Throughput Image Analysis of Fibrillar Materials: A case study on polymer nanofiber packing, alignment, and defects in organic field effect transistors. *ACS Appl. Mater. Interfaces* **2017**, *9* (41), 36090−36102.
(39) Thomas, D. Pygix. https://github.com/tgdane/pygix (accessed 4 29, 2024).
(40) Ashiotis, G.; Deschildre, A.; Nawaz, Z.; Wright, J. P.; Karkoulis, D.; Picca, F. E.; Kieffer, J. The fast azimuthal integration Python library:pyFAI. *J. Appl. Crystallogr.* **2015**, *48* (2), 510−519.
(41) Kieffer, J.; Valls, V.; Blanc, N.; Hennig, C. New tools for calibrating diffraction setups. *J. Synchrotron Radiat.* **2020**, *27* (2), 558−566.
(42) Clark, J.; Chang, J.-F.; Spano, F. C.; Friend, R. H.; Silva, C. Determining Exciton Bandwidth and Film Microstructure in Polythiophene Films Using Linear Absorption Spectroscopy. *Appl. Phys. Lett.* **2009**, *94*, 163306.
(43) Tsoi, W. C.; James, D. T.; Kim, J. S.; Nicholson, P. G.; Murphy, C. E.; Bradley, D. D. C.; Nelson, J.; Kim, J.-S. The nature of In-Plane Skeleton Raman modes of P3HT and their correlation to the degree of molecular order in P3HT:PCBM blend thin films. *J. Am. Chem. Soc.* **2011**, *133* (25), 9834−9843.
(44) Gierschner, J.; Huang, Y.-S.; Van Averbeke, B.; Cornil, J.; Friend, R. H.; Beljonne, D. Excitonic versus electronic couplings in molecular assemblies: The importance of non-nearest neighbor interactions. *J. Chem. Phys.* **2009**, *130* (4), 044105.
(45) Niles, E. T.; Roehling, J. D.; Yamagata, H.; Wise, A. J.; Spano, F. C.; Moulé, A. J.; Grey, J. K. J-Aggregate behavior in poly-3-hexylthiophene nanofibers. *J. Phys. Chem. Lett.* **2012**, *3* (2), 259−263.
(46) Zhang, G.; Lee, S.; Gutiérrez-Meza, E.; Buckley, C.; McBride, M.; Valverde-Chávez, D. A.; Kwon, Y. H.; Savikhin, V.; Xiong, H.; Dunn, T. J.; Toney, M. F.; Yuan, Z.; Silva, C.; Reichmanis, E. Robust and stretchable polymer semiconducting networks: from film microstructure to macroscopic device performance. *Chem. Mater.* **2019**, *31* (17), 6530−6539.
(47) Clark, J.; Silva, C.; Friend, R. H.; Spano, F. C. Role of Intermolecular Coupling in the Photophysics of Disordered Organic Semiconductors: Aggregate Emission in Regioregular Polythiophene. *Phys. Rev. Lett.* **2007**, *98* (20), 206406.
(48) Spano, F. C. Modeling Disorder in Polymer Aggregates: The Optical Spectroscopy of Regioregular Poly(3-Hexylthiophene) Thin Films. *J. Chem. Phys.* **2005**, *122* (23), 234701.
(49) Kuebler, J.; Dhapola, S.; Fernandez-Ballester, L. Selecting for Surface-Induced vs Bulk Crystallization in P3HT Thin Films: Distinct Morphology, Orientation, and Linear Growth Rates. *Macromolecules* **2024**, *57* (6), 2639−2650.
(50) Reinspach, J. A.; Diao, Y.; Giri, G.; Sachse, T.; England, K.; Zhou, Y.; Tassone, C.; Worfolk, B. J.; Presselt, M.; Toney, M. F.; Mannsfeld, S.; Bao, Z. Tuning the morphology of Solution-Sheared P3HT:PCBM films. *ACS Appl. Mater. Interfaces* **2016**, *8* (3), 1742−1751.
(51) Spano, F. C. Absorption in regio-regular poly(3-hexyl)-thiophene thin films: Fermi resonances, interband coupling and disorder. *Chem. Phys.* **2006**, *325* (1), 22−35.
(52) Zheng, Y.; Venkatesh, R.; Callaway, C. P.; Viersen, C.; Fagbohungbe, K. H.; Liu, A. L.; Risko, C.; Reichmanis, E.; Silva-Acuña, C. Chain conformation and exciton delocalization in a Push-Pull conjugated polymer. *Chem. Mater.* **2023**, *35* (23), 10258−10267.
(53) Korevaar, P. A.; De Greef, T. F. A.; Meijer, E. W. Pathway complexity in π-Conjugated materials. *Chem. Mater.* **2014**, *26* (1), 576−586.
(54) Kayunkid, N.; Uttiya, S.; Brinkmann, M. Structural model of regioregular poly(3-hexylthiophene) obtained by electron diffraction analysis. *Macromolecules* **2010**, *43* (11), 4961−4967.
(55) Bittle, E. G.; Ro, H. W.; Snyder, C. R.; Engmann, S.; Kline, R. J.; Zhang, X.; Jurchescu, O. D.; DeLongchamp, D. M.; Gundlach, D. J. Dependence of electrical performance on structural organization in polymer field effect transistors. *J. Polym. Sci., Part B:Polym. Phys.* **2017**, *55* (14), 1063−1074.
(56) Chang, M.; Lee, J.; Kleinhenz, N.; Fu, B.; Reichmanis, E. Photoinduced anisotropic supramolecular assembly and enhanced charge transport of poly(3-hexylthiophene) thin films. *Adv. Funct. Mater.* **2014**, *24* (28), 4457−4465.
(57) Chang, M.; Choi, D.; Wang, G.; Kleinhenz, N.; Persson, N.; Park, B.; Reichmanis, E. Photoinduced anisotropic assembly of conjugated polymers in insulating polymer blends. *ACS Appl. Mater. Interfaces* **2015**, *7* (25), 14095−14103.
(58) Park, K. S.; Kwok, J. J.; Dilmurat, R.; Qu, G.; Kafle, P.; Luo, X.; Jung, S.-H.; Olivier, Y.; Lee, J.-K.; Mei, J.; Beljonne, D.; Diao, Y.

https://doi.org/10.1021/acs.chemmater.4c03392
Chem. Mater. 2025, 37, 2795−2805

Tuning conformation, assembly, and charge transport properties of conjugated polymers by printing flow. *Sci. Adv.* **2019**, *5* (8), No. eaaw7757.

NOTE ADDED AFTER ASAP PUBLICATION

This article published ASAP on April 2, 2025. The first sentence in the Film Deposition paragraph of the Experimental Section has been updated. The caption of Figure 5a was also updated and the revised version reposted on April 3, 2025.

https://doi.org/10.1021/acs.chemmater.4c03392
Chem. Mater. 2025, 37, 2795−2805